Superconductivity competing with the incommensurate antiferromagnetic insulating state in the organic conductor (MDT-TS)$(AuI_2)_{0.441}$

Tadashi Kawamoto, Yoshimasa Bando, and Takehiko Mori
Department of Organic and Polymeric Materials, Graduate School of Science and Engineering, Tokyo Institute of Technology, O-okayama, Meguro-ku, Tokyo 152-8552, Japan

Kazuo Takimiya and Tetsuo Otsubo
Department of Applied Chemistry, Graduate School of Engineering, Hiroshima University, Kagamiyama, Higashi-Hiroshima, Hiroshima 739-8527, Japan

(Received 15 November 2004; published 4 February 2005)

The organic conductor (MDT-TS)$(AuI_2)_{0.441}$ undergoes a metal-insulator transition at $T_{MI}=50$ K, where MDT-TS is 5*H*-2-(1,3-diselenol-2-ylidene)-1,3,4,6-tetrathiapentalene. The static magnetic susceptibility demonstrates an antiferromagnetic ordering below this temperature. Hydrostatic pressure suppresses this insulating state, and a superconductivity appears at $T_c=3.2$ K above 10.5 kbar. The phase diagram demonstrates a transition from the incommensurate antiferromagnetic insulating state to a superconducting state in an organic conductor with a noninteger carrier number.

DOI: 10.1103/PhysRevB.71.052501 PACS number(s): 74.70.Kn, 71.30.+h, 74.25.Ha

In the strongly correlated electron materials including the copper-oxide (high-T_c) superconductors,[1] heavy fermion compounds,[2] and organic molecular crystals,[3–5] the superconducting phases appear in the vicinity of the antiferromagnetic state. In view of the current theoretical models, the superconductivity in these materials is possibly mediated by the spin fluctuations.[6] Organic superconductors such as $(TMTSF)_2X$ (TMTSF: tetramethyl-tetraselenafulvalene, *X*: anions) and κ-$(ET)_2X$ [ET: bis(ethylenedithio)tetrathiafulvalene] have superconducting phases bordering on spin density wave (SDW) or antiferromagnetic insulating states in the temperature-pressure (*T*-*P*) phase diagrams. It is characteristic of these organic superconductors that the ratio of the donor molecules to anions is stoichiometric 2:1, and the carrier number is fixed to one hole per two donor molecules. The donor molecules form dimerized structures, and the resulting 3/4-filled band in the presence of the dimerization gap corresponds to effective half filling. The ground state of these organic superconductors is regulated by U/W, where U is the on-site Coulomb repulsion and W is the bandwidth. Accordingly, the ground state depends not only on physical pressure but also on the change of the anion *X* (chemical pressure).

By contrast, an ambient-pressure organic superconductor (MDT-TSF)$(AuI_2)_{0.436}$, where MDT-TSF is methylenedithio-tetraselenafulvalene [Fig. 1(a)], has uniform donor stacking without dimerization, and the anions form chains running parallel to the donor stacks.[7] The anion periodicity is incommensurate to the donor spacing, and the noninteger composition has been determined from the ratio of the donor lattice ($a=4.016$ Å) and the anion lattice ($a'=9.221$ Å) as $a/a'=0.436$.[8] Therefore, the energy band is not effective half filling. The Fermi surface is two-dimensional (2D) owing to the considerable interchain interaction, and the existence of closed orbits has been verified by the observation of the Shubnikov–de Haas oscillations together with the characteristic reconstruction due to the incommensurate anion potential.[9] The salts of the sulfur analog MDT-ST, where MDT-ST is 5*H*-2-(1,3-dithiol-2-ylidene)-1,3-diselena-4,6-dithiapentalene [Fig. 1(a)], have similar incommensurate structures, and also show superconductivity at ambient pressure.[10]

Recently, we have developed another sulfur derivative (MDT-TS)$(AuI_2)_{0.441}$ [Fig. 1(a)], which has basically the same crystal structure [Figs. 1(b) and 1(c)], but exhibits a metal-insulator transition at low temperatures.[11] The tight-binding energy band of these compounds, without the incommensurate anion potential, is expressed as the following equation:

$$E(k_a,k_b) = \pm 2\sqrt{(t_{p1}+t_{p2})^2 - 4t_{p1}t_{p2}\sin^2(k_a a/2)}\cos(k_b b/2) + 2t_a\cos(k_a a). \quad (1)$$

The transfer integrals t_i, defined in Fig. 1(b), are estimated from the intermolecular overlap integrals S_i as $t_i=E\times S_i$ in which the energy level of the highest occupied molecular orbital (HOMO) E is taken to be −10 eV. The overlap integrals are calculated on the basis of the extended Hückel method.[12] We have calculated the overlap integrals without S 3*d* and Se 4*d* orbitals on the basis of the results of (MDT-TSF)$(AuI_2)_{0.436}$ reported in Ref. 9. The calculated transfer integrals of the present compound are $t_a=76$, $t_{p1}=-7.9$, and $t_{p2}=-26.3$ meV. Owing to the sulfur substitution, the total bandwidth, $W=4t_a+2|t_{p1}+t_{p2}|+2|t_{p1}-t_{p2}|$, of (MDT-TS)$(AuI_2)_{0.441}$ is 26% smaller than that of (MDT-ST)$(I_3)_{0.417}$. Therefore, the electronic correlation of this compound is strongest among these conductors. The calculated Fermi surface [Fig. 1(d)] is, however, a 2D one not much different from the superconducting selenium analogs.

The present paper reports discovery of superconductivity in this compound under pressure as well as the investigations of the *T*-*P* phase diagram and the ground state at ambient pressure. This work elucidates for the first time a transition from an insulating state to a superconducting state in an in-

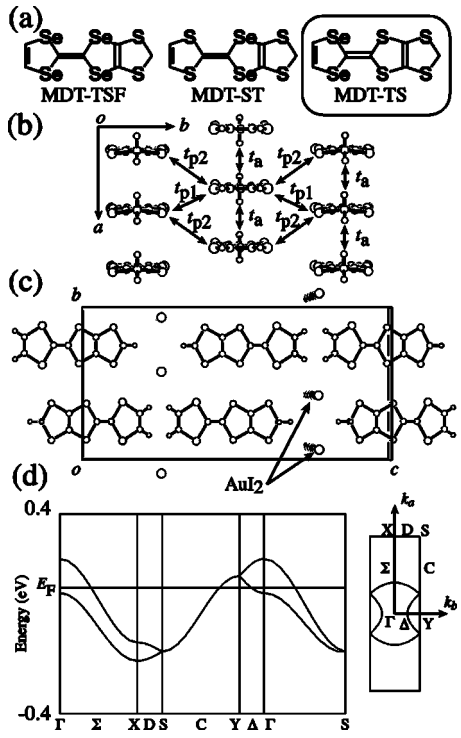

FIG. 1. (a) MDT-TSF series molecules. (b) Crystal structure projected along the molecular long axis and (c) projection onto the *bc* plane of $(MDT\text{-}TS)(AuI_2)_{0.441}$. (d) The energy band structure and the Fermi surface.

commensurate (non integer carrier number) organic superconductor.

Single crystals were prepared by the electrocrystallization.[11] Electrical resistivity was measured by the four-probe method along the *a* axis with ac current (usually 100 μA) down to 1.5 K. The high-pressure resistivity measurements were carried out by the conventional clamp cell technique. Because the pressure is released by about 1.5 kbar between 300 K and 50 K, this value has been subtracted from room-temperature values.[13] Thermoelectric power measurement was carried out by the two terminal method along the *a* and *b* axes down to 2.0 K. For the magnetoresistance measurements, the sample was mounted on a cryostat in a 9 T superconducting magnet, and was cooled to 1.5 K. The static magnetic susceptibility was measured by a SQUID magnetometer under the magnetic field of $H=10$ kOe. The measurements were carried out for aligned crystals [2.06(5) mg] under the fields of $H\|a$ and $H\|b$. The spin susceptibilities were obtained after the subtraction of Pascal's law, $\chi_{dia}=-4.70\times10^{-4}$ emu/mol, where we define 1 mol as $(MDT\text{-}TS)_{2.27}(AuI_2)$.

Figure 2 shows the *a*-axis resistivity (ρ) and thermopowers ($Q_{\|a}$ and $Q_{\|b}$) at ambient pressure. The resistivity decreases with decreasing temperature and increases below $T_\rho=85$ K. The metal-insulator transition temperature T_{MI} is determined from the peak of $d(\ln\rho)/d(1/T)$ as $T_{MI}=50$ K. The charge gap estimated from the slope of the Arrhenius plots is $\Delta\approx710$ K at T_{MI}. The charge gap strongly depends on the temperature and decreases to $\Delta\approx36$ K around 10 K. The thermopowers show that the carriers are holes and

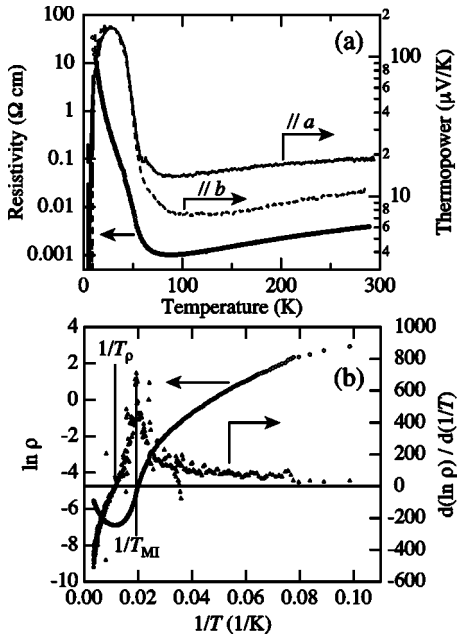

FIG. 2. (a) Resistivity and thermopower of $(MDT\text{-}TS)(AuI_2)_{0.441}$. (b) The definition of T_ρ and T_{MI} by the resistivity data.

slightly anisotropic in the conducting sheet (the *ab* plane). The thermopower also exhibits metallic behavior above $T_\rho=85$ K and shows semiconducting behavior below 85 K. The first derivative of the semiconducting plot of the thermopower, $dQ/d(1/T)$, also gives us the same values of T_ρ and T_{MI}.

High-pressure resistivities are shown in Fig. 3(a). T_ρ and T_{MI} shift to lower temperatures as the pressure increases, and the resistivities drop to the noise level above $P_c=10.5$ kbar below onset $T_c=4.3$ K (midpoint $T_c=3.2$ K). These resistivity drops indicate a superconducting transition, because the drops are suppressed by magnetic fields [Figs. 3(b) and 3(c)]. Figures 3(b) and 3(c) show that the resistance peak corresponds to the onset T_c. The resistance peak does not disappear in the measured pressure region, and T_c increases with increasing pressure (midpoint $T_c=4.4$ K at 11.9 kbar). In the region $T_c<T<T_\rho$, negative magnetoresistance was observed as shown in Figs. 3(b) and 3(c).

Figure 4 shows the static magnetic susceptibility (χ_a and χ_b). The value of the spin susceptibility at room temperature is 5.9×10^{-4} emu/mol. In spite of the decreasing resistivity at high temperatures, the spin susceptibility gradually increases with decreasing temperature, indicating a strongly correlated state. To the best of our knowledge, there is no organic conductor showing decreasing resistivity together with increasing susceptibility. Both χ_a and χ_b have a broad peak at 75 K (7.5×10^{-4} emu/mol) and decrease below this temperature. This temperature dependence is, however, neither well reproduced by the one-dimensional (1D) Heisenberg model, the 2D square lattice model, nor the 2D triangular lattice model. The results fitted to these three antifferomagnet models ($S=1/2$) are depicted in Fig. 4.[14–16] The temperature dependence of the magnetic susceptibility is weaker than these models and is intermediate of the itinerant

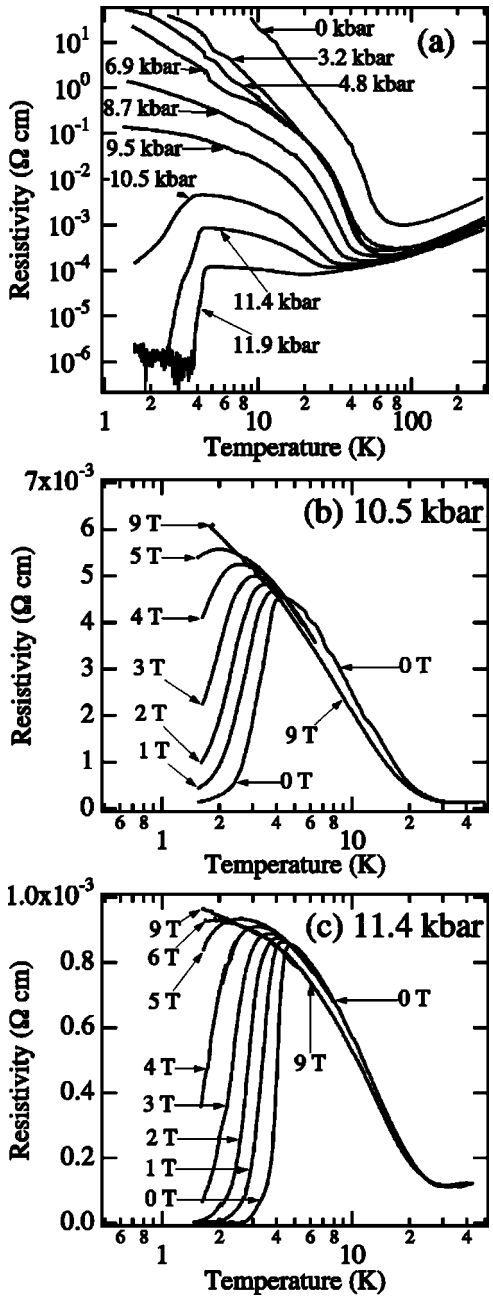

FIG. 3. (a) Temperature dependence of the resistivities under various pressures. (b) Resistivities under various magnetic fields at 10.5 kbar and (c) at 11.4 kbar.

and localized states. The magnetic susceptibility shows anisotropic behavior below the antiferromagnetic transition at T_N=50 K (Fig. 4). This temperature agrees with the metal-insulator transition temperature T_{MI} observed in the resistivity. The easy axis corresponds to the crystallographic *b* axis. The temperature at which the susceptibility has a peak is close to T_ρ, suggesting that the resistivity minimum is potentially associated with the magnetic fluctuations above T_{MI}.

Figure 5 shows the *T*-*P* phase diagram of $(\mathrm{MDT\text{-}TS})(\mathrm{AuI_2})_{0.441}$ based on the transport and the magnetic measurements. We can locate ambient-pressure state of the MDT-TSF and MDT-ST superconductors above 12 kbar

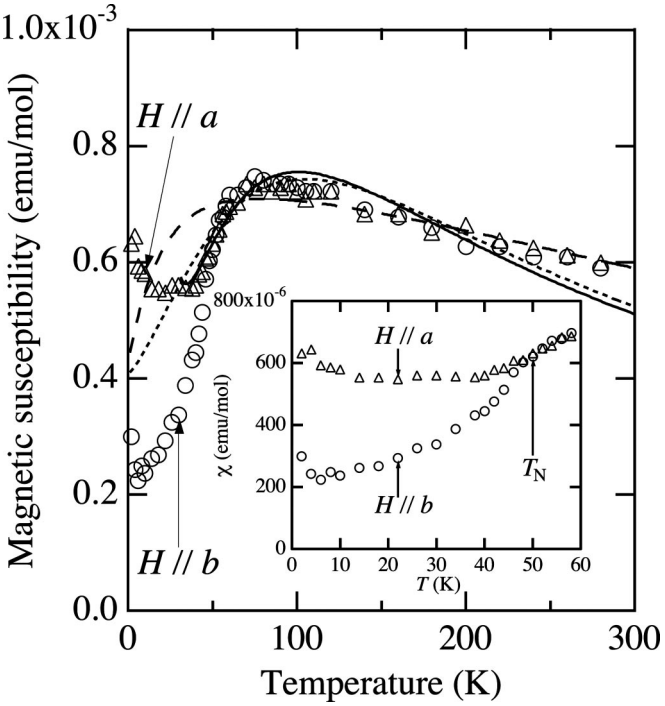

FIG. 4. Temperature dependence of the static magnetic susceptibilities ($H\|a$ and $H\|b$). The dotted line is the 1D Heisenberg model (J=−85 K and $\mu_{\mathrm{eff}}=0.76\mu_B$), the solid line is the 2D square lattice model (J=−110 K and $\mu_{\mathrm{eff}}=0.77\mu_B$), and the dashed line is the 2D triangular lattice model (J=−209 K and $\mu_{\mathrm{eff}}=1.1\mu_B$) fitted to the observed data of $H\|b$, under g=2.0. The inset shows the data in the low-temperature region.

of this phase diagram. Although this phase diagram resembles that of $(\mathrm{TMTSF})_2X$,[3,5] T_{MI} and T_c of the present compound are about four times higher than those of $(\mathrm{TMTSF})_2X$. The magnetic insulating state below T_{MI} =50 K is not a simple antiferromagnetic state with alternate spins such as κ-$(\mathrm{ET})_2X$, because each molecule or dimer does not have one electron. In this sense, the insulating state is regarded as a kind of SDW state. In contrast to

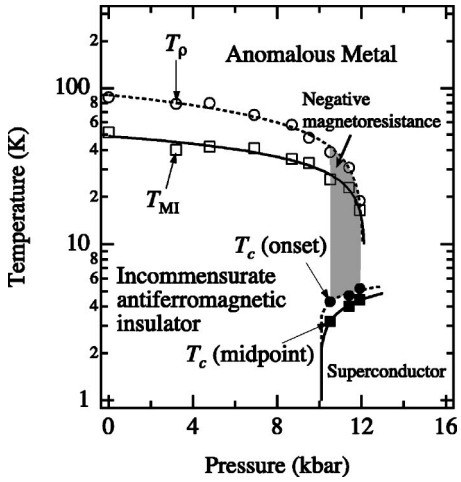

FIG. 5. The phase diagram of $(\mathrm{MDT\text{-}TS})(\mathrm{AuI_2})_{0.441}$. The solid and dotted lines are guides to the eye.

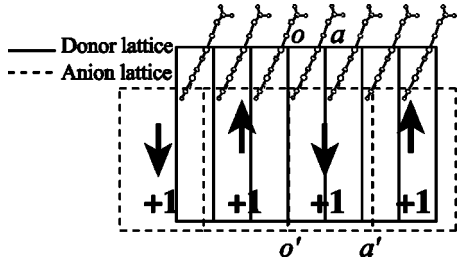

FIG. 6. Schematic drawing of the incommensurate antiferromagnetic insulator.

$(TMTSF)_2X$, however, the electronic state of the present compound is two dimensional [Fig. 1(d)], and the Fermi surface does not nest. Moreover, the effective Bohr magneton, $>0.7\mu_B$, is much larger than that of the typical SDW ordering ($\sim 0.1\mu_B$).[5]

This new electronic state is naively understood by assuming a localized state that is incommensurate to the donor sites. As shown in Fig. 6, each 2.27 (inverse of 0.441) donor molecules have one hole. On account of the strong correlation, the electron is localized, and undergoes an antiferromagnetic transition. The insulating state is symbolically called "incommensurate antiferromagnetic insulating state." In the $(TMTSF)_2X$ and κ-$(ET)_2X$ series, the importance of dimerization and the effectively half-filled situation has been emphasized for a long time, but a similar phase diagram appears in the present compound in spite of the noninteger carrier number.

If we take account of the incommensurate anion potential, the resulting subband of the present compound is effective half filling. Nonetheless this state is not simply understood as the $4k_F$ state in a 1D system, because the present system is entirely 2D. Furthermore, only the effect of U cannot make the system insulating, but the influence of the nearest-neighbor Coulomb repulsion V (the extended Hubbard model) is necessary.[17,18] In this sense, the "incommensurate antiferromagnetic insulating state" is a kind of charge ordered state. The present phase diagram demonstrates that the incommensurate electron localizes to a charge ordered state without particular assistance of dimerization or U, and even undergoes an antiferromagnetic transition. Furthermore, there is even a possibility that the superconducting state is associated with the incommensurate antiferromagnetic fluctuation.

In summary, $(MDT\text{-}TS)(AuI_2)_{0.441}$ is the first incommensurate organic system that shows a transition from an "incommensurate antiferromagnetic insulating state" to a superconducting phase at 3.2 K under 10.5 kbar. The precise description of this new localized state will also be related to the symmetry of the superconducting state.

The authors thank Professor H. Fukuyama for the concept of the "incommensurate antiferromagnetic insulator." This work was partially supported by a Grant in Aid for Scientific Research (Grant Nos. 14740377, 15073211, and 15073218) from the Ministry of Education, Science, Sports and Culture.

[1] G. Burns, *High-Temperature Superconductivity* (Academic Press, New York, 1992).
[2] N. D. Mathur, F. M. Grosche, S. R. Julian, I. R. Walker, D. M. Freye, R. K. W. Haselwimmer, and G. G. Lonzarich, Nature (London) **394**, 39 (1998).
[3] D. Jérome, Science **252**, 1509 (1991).
[4] K. Kanoda, Hyperfine Interact. **104**, 235 (1997).
[5] T. Ishiguro, K. Yamaji, and G. Saito, *Organic Superconductors*, 2nd ed. (Springer, Berlin, 1998).
[6] S.-C. Zhang, Science **275**, 1089 (1997).
[7] K. Takimiya, Y. Kataoka, Y. Aso, T. Otsubo, H. Fukuoka, and S. Yamanaka, Angew. Chem., Int. Ed. **40**, 1122 (2001); K. Takimiya, M. Kodani, Y. Kataoka, Y. Aso, T, Otsubo, T. Kawamoto, and T. Mori, Chem. Mater. **15**, 3250 (2003).
[8] T. Kawamoto, T. Mori, K. Takimiya, Y. Kataska, Y. Aso, and T. Otsubo, Phys. Rev. B **65**, 140508(R) (2002).
[9] T. Kawamoto, T. Mori, C. Terakura, T. Terashima, S. Uji, K. Takimiya, Y. Aso, and T. Otsubo, Phys. Rev. B **67**, 020508(R) (2003); T. Kawamoto, T. Mori, C. Terakura, T. Terashima, S. Uji, H. Tajima, K. Takimiya, Y. Aso, and T. Otsubo, Eur. Phys. J. B **36**, 161 (2003).
[10] K. Takimiya, A. Takamori, Y. Aso, T. Otsubo, T. Kawamoto, and T. Mori, Chem. Mater. **15**, 1225 (2003); T. Kawamoto, T. Mori, T. Terashima, S. Uji, H. Kitagawa, K. Takimiya, A. Takamori, and T. Otsubo, J. Phys. IV **114**, 517 (2004).
[11] K. Takimiya, M. Kodani, N. Niihara, Y. Aso, T. Otsubo, Y. Bando, T. Kawamoto, and T. Mori, Chem. Mater. **16**, 5120 (2004).
[12] T. Mori, A. Kobayashi, Y. Sasaki, H. Kobayashi, G. Saito, and H. Inokuchi, Bull. Chem. Soc. Jpn. **57**, 627 (1984).
[13] K. Murata, H. Yoshino, H. O. Yadav, Y. Honda, and N. Shirakawa, Rev. Sci. Instrum. **68**, 2490 (1997).
[14] J. C. Bonner and M. E. Fisher, Phys. Rev. **135**, A640 (1964); W. E. Hatfield, R. R. Weller, and J. W. Hall, Inorg. Chem. **19**, 3825 (1980).
[15] M. E. Lines, J. Phys. Chem. Solids **31**, 101 (1970).
[16] M. Tamura and R. Kato, J. Phys.: Condens. Matter **14**, L729 (2002).
[17] F. Mila, Phys. Rev. B **49**, R14 047 (1994).
[18] H. Seo, J. Phys. Soc. Jpn. **69**, 805 (2000).